



Efficient visible-light-driven depolymerization of oxidized lignin to aromatics catalyzed by an iridium complex immobilized on mesocellular silica foams



Zhongkai Hao^a, Shuyuan Li^a, Jiarong Sun^b, Song Li^a, Fang Zhang^{a,*}

^a The Education Ministry Key Lab of Resource Chemistry, Shanghai Key Laboratory of Rare Earth Functional Materials, Shanghai Normal University, Shanghai 200234, China

^b Han Academy, 33-35 Wong Chuk Hang Road, Hong Kong

ARTICLE INFO

Keywords:

Lignin depolymerization
Visible-light photocatalysis
 $\text{Ir}(\text{ppy})_2(\text{bpy})$ -MCFs photocatalyst
Mesoporous cellular silica foams
Click chemistry

ABSTRACT

A novel $\text{Ir}(\text{ppy})_2(\text{bpy})$ complex-containing mesoporous cellular silica foams ($\text{Ir}(\text{ppy})_2(\text{bpy})$ -MCFs) was prepared by a facile thiol-ene click reaction between the prefabricated thiol-functionalized mesoporous cellular silica foams and vinyl-tagged $[\text{Ir}(\text{ppy})_2(\text{bpy})]\text{PF}_6$ complex. The elaborate $\text{Ir}(\text{ppy})_2(\text{bpy})$ -MCFs material possessed the large surface area ($355 \text{ cm}^2/\text{g}$), open foam-like mesoporous structure with 30 nm cell pore size and 3.0 nm window pore size. Importantly, it had the well-defined molecular configuration of $\text{Ir}(\text{ppy})_2(\text{bpy})$ active species. As expected, it exhibited excellent catalytic reactivity and selectivity in the visible-light-driven reductive depolymerization of oxidized lignin β -O-4 model compounds including *p*-hydroxyphenyl (H)-, guaiacyl (G)- and syringyl (S)-type units under the mild conditions. Meanwhile, it showed the comparable catalytic efficiency with the corresponding homogeneous $[\text{Ir}(\text{ppy})_2(\text{bpy})]\text{PF}_6$ catalyst. These high catalytic performances could be attributed to aerogel-like three-dimensional pore structure and high visible-light transparency, which efficiently decreased the mass transfer resistance and the photon propagation hindrance. Furthermore, it could be easily recycled and reused at least six times without the remarkable loss of catalytic activity.

1. Introduction

The use of fossil resources as the raw materials for the production of fuels and chemicals causes the ever-increasing environmental pressure [1]. Accordingly, the non-edible, abundant and cheap lignocellulosic biomass as an alternative feedstock attracts much attention due to their renewable and carbon-neutral properties [2]. In the context, lignin is one of the most abundant biomass and also is the unique aromatic-based biopolymer that accounts for almost 30% organic carbon on Earth. However, due to the byproduct in the pulp and paper industry, it is usually treated as the waste and mostly used as the low-value fuel that is burned to produce heat and energy [3,4]. This manufacturing process imposes a direct negative impact on resource utilization and environmental protection [5]. To address this dilemma, the depolymerization of lignin for the production of bulk or functionalized aromatic chemicals is recognized as a valuable strategy because it can provide the promising alternatives to the commonly used petroleum-based starting materials [6–12]. Nevertheless, the development of an efficient and viable transformation of lignin into the chemicals still remains a great challenge due to the robustness and complexity of its three-dimensional structure [13].

Lignin is composed of three monolignol units, coniferyl, coumaryl and sinapyl alcohols, randomly connected by various types of ether and C–C linkages [14]. One approach of lignin depolymerization is to cleave the C–O bonds of the β -O-4 ethers that constitute 45–60% of the linkage structures [15]. Accordingly, the controlled cleavage of β -O-4 linkage is believed as an attractive route for converting lignin into value-added aromatic products. Generally, a two-step oxidation and reduction protocol is used based on the first selective oxidation of the α - or γ -carbon in the benzylic β -O-4 alcohol to benzylic β -O-4 ketone, which can weaken the C–O bonds of β -O-4 linkages. Subsequently, the C–O bonds of the benzylic β -O-4 ketones are broken by the second reduction treatment, giving the complementary fragmentation partners [16]. In this approach, the chemoselective aerobic oxidation of β -O-4 alcohol to β -O-4 ketone was already well demonstrated by Stahl group [17]. But, the reduction step generally requires high temperature and/or high pressure, which are not well for the functional groups tolerance such as free phenols and γ -alcohols. Therefore, the mild and selective reduction of the oxidized lignin is urgently needed [18].

Visible-light-driven photoredox catalysis has been proven as a reliable and powerful tool to promote organic transformations under the

* Corresponding author.

E-mail address: zhangfang@shnu.edu.cn (F. Zhang).

mild conditions due to its abundance, non-pollution and cleanliness [19]. Recently, this strategy was extended to de-polymerize lignin models or extracts by using transition-metal complexes, inorganic semiconductors or π -conjugated porous organic frameworks as the photocatalysts reported by Stephenson, Xie, Wang and Zhang groups, respectively [20–24]. In particular, the Iridium-based metal complexes exhibited the superior catalytic performances because of their strong visible light absorption, long life-time of the excited species and well-defined molecular structure. But, the expensive price, limited amount on Earth associated with difficult isolation and recycle impede its future application. Thus, the immobilization of the homogeneous Iridium complex onto solid supports without any loss of catalytic activity needs to be developed. Until now, several groups have already demonstrated the successful immobilization of Iridium complex onto different supports such as silica, polymer and metal-organic framework by post-grafting, cross-linking or direct encapsulation approach [25–34]. However, none of them have been explored for the depolymerization of lignin, which is probably due to that their pore sizes are too small to compatible with large molecular size of lignin.

Mesoporous cellular silica foams (MCFs) have aerogel-like three-dimensional (3D) pore channels with large spherical cell pores interconnected with window pores. Interestingly, the average pore size of MCFs can be controlled in the range of 5–50 nm and the specific surface area is up to 1000 m²/g. Also, it displays the high hydrothermal stability [35]. These unique properties make it good candidate for catalytic application, especially for the reactants with large size [36–39]. Moreover, the 3D porous structure and high transparency for visible light are advantageous for photocatalysis application. For example, TiO₂ nanoparticles were incorporated into the pore channels of MCFs reported by Choi and Zhang groups [40,41]. These catalysts showed the enhanced photocatalytic activity both in the hydroxylation reactions and pollutant degradation. Herein, we reported for the first preparation of Ir(ppy)₂(bpy) complex-containing MCFs by reacting thiol-functionalized MCFs with the vinyl-tagged [Ir(ppy)₂(bpy)]PF₆ complex via a simple thiol-ene click reaction. The as-prepared Ir(ppy)₂(bpy)-MCFs exhibited the large surface area and big pore size. Meanwhile, the molecular configuration of Ir(ppy)₂(bpy) complex can be well-retained. As a result, it can serve as an efficient photocatalyst for the depolymerization of oxidized lignin β -O-4 model compounds under visible light illumination. Moreover, it can be easily recycled and reused for at least six times without the significant loss of activity.

2. Experimental

2.1. Preparation of thiol-functionalized mesocellular silica foams (SH-MCFs)

In a typical protocol, the P123 surfactant (EO₂₀PO₇₀EO₂₀, 4.0 g) was added into aqueous hydrochloric acid solution (150 mL, 1.60 mol/L) and stirred at 30 °C for 2.0 h. Then, ammonium fluoride (46 mg) and mesitylene (4.60 mL) were mixed with the solution and stirred for another 1.0 h. After that, TEOS (Tetraethoxysilane, 7.34 mL) was added and allowed to pre-hydrolyze for 1.0 h at 40 °C and subsequently a certain amount of MPTMS (3-Mercaptopropyltrimethoxysilane) was added dropwise. After stirring for 20 h, the mixture was transferred into a Teflon bottle at 100 °C for 24 h. The resulting product was filtered off, washed with water and ethanol and dried in vacuum at 80 °C for 12 h. Finally, the solid sample was immersed into ethanol solution and refluxed under 80 °C for 12 h to remove the P123 surfactant. The as-received samples were denoted as SH-MCFs-1, SH-MCFs-2 and SH-MCFs-3, which corresponded to the 10%, 20%, 30% molar percentage of MPTMS/(MPTMS + TEOS), respectively.

2.2. Synthesis of vinyl-tagged [Ir(ppy)₂(bpy)]PF₆ complex

Diisopropylamine (0.80 mL) and n-BuLi/hexane solution (3.50 mL)

were mixed in 10 mL anhydrous THF and allowed to stir at –78 °C under N₂ atmosphere for 1.0 h. Afterward, the mixture of 1.0 g 4,4'-Dimethyl-2,2'-dipyridyl and 45 mL anhydrous THF was added via syringe and stirred at –78 °C for 15 min and then stirred at 0 °C for another 1.0 h. Then, a solution of 0.72 g allyl bromide solved in 15 mL anhydrous THF was added by syringe and continued to stir at 25 °C for 12 h. Then, 5.0 mL MeOH was added to the mixture and dried under reduced pressure at 5–10 °C to obtain the crude product. This product was dissolved in CH₂Cl₂ (5.0 mL), washed by deionized water (20 mL) and saturated brine (20 mL, 26.5 wt %) and then the achieved organic layer was dried with MgSO₄. The organic extracts were concentrated in vacuum, and the residue were purified by chromatography to afford the product (99 mg) and Dichlorotetrakis[2-(2-pyridyl)phenyl]diiridium(III) (214 mg) were added in ethylene glycol (10 mL) and stirred at 150 °C under N₂ atmosphere for 15 h. After cooling to room temperature, the solution was extracted with deionized water (150 mL) and diethyl ether (50 mL) for three times. Finally, NH₄PF₆ solution (1.0 g/10 mL deionized water) was added to the organic layer, stirred at 65 °C until the precipitate appeared. The obtained precipitate was washed by ethanol and dried in vacuum to give the final product.

2.3. Fabrication of Ir(ppy)₂(bpy) complex-containing mesocellular silica foams (Ir(ppy)₂(bpy)-MCFs)

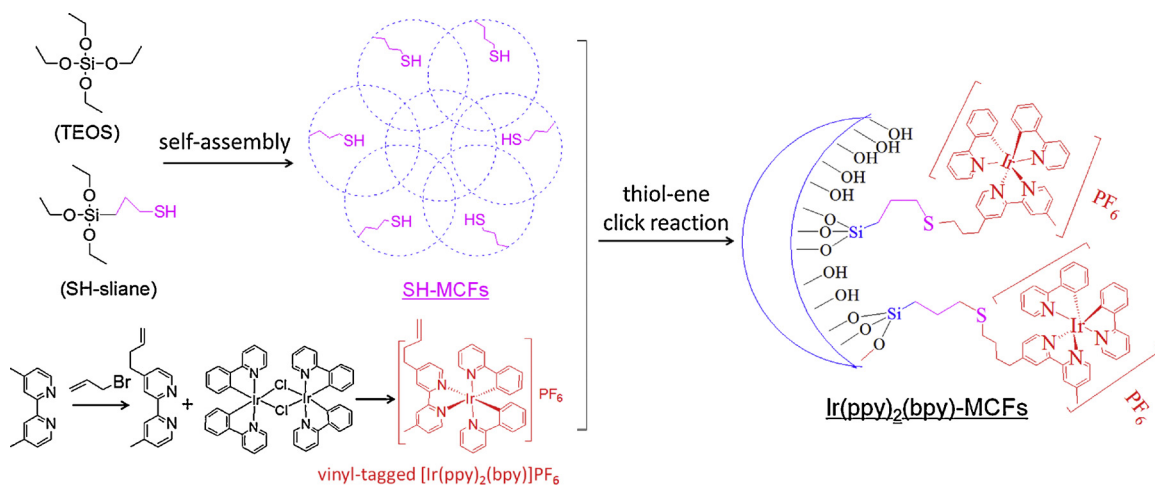
In a typical synthesis, the as-prepared vinyl-tagged [Ir(ppy)₂(bpy)]PF₆ complex (50 mg) and SH-MCFs-2 (100 mg) were dispersed in 10.0 mL CHCl₃. Then, 20 mg AIBN (azodiisobutyronitrile) as the initiator was added in the solution. After ultrasound for 0.5 h, the mixture was refluxed 24 h under N₂ atmosphere. The product was filtrated, washed by ethanol for three times to remove un-reacted Iridium species on the support and dried in vacuum at 80 °C for 12 h.

2.4. Characterization

The Iridium loading was calculated by inductively coupled plasma optical emission spectrometer. Fourier transform infrared (FT-IR) spectra were obtained on a Nicolet Magna 550 spectrometer. Thermal gravimetric analysis (TGA) was performed with a Perkin-Elmer Pyris Diamond TG analyzer with a heating ramp of 2.0 °C/min in 50 mL/min of air flow. The surface electronic states were analyzed by X-ray photoelectron spectroscopy (XPS, Perkin-Elmer PHI 5000C ESCA). All the binding energy values are calibrated by using C1s = 284.6 eV as a reference. UV-vis diffuse reflectance spectra (UV-vis DRS) were collected on a Shimadzu UV22550 spectrometer. Nitrogen sorption isotherms were measured at 77 K on a Quantachrome NOVA 4000e analyzer, from which the specific surface area was calculated by multiple-point Brunauer-Emmett-Teller (BET) model. The average pore sizes of the cell and the window in the MCFs were calculated from the adsorption isotherms and the desorption isotherms, respectively, by using Barrett-Joyner-Halenda (BJH) model. Transmission electron microscopy (TEM) images were observed on a JEM-2011 at an acceleration voltage of 200 kV.

2.5. Activity test

In a typical depolymerization reaction of lignin β -O-4 model compound, 2-(2-methoxyphenoxy)-1-(4-methoxyphenyl)ethanone (0.50 mmol), DIPEA (*N,N*-Diisopropylethylamine, 1.5 mmol), HCOOH (1.5 mmol), MeCN (5.0 mL) and 1.0 mol% Ir(ppy)₂(bpy)-MCFs catalyst were mixed in a 10 mL three-necked round-bottomed flask. After reacting at 25 °C for 6.0 h under mild stirring by Xenon lamp (> 420 nm) as the visible light source, the products were extracted with methanol, followed by analysis on liquid chromatography (LC, Agilent 1260) equipped with a ZORBAX Eclipse XDB-C18 column with the mesitylene as the internal standard. The reproducibility is checked by repeating each result at least three times and is found to be within \pm 5%.



Scheme 1. Schematic picture of the preparation of $\text{Ir}(\text{ppy})_2(\text{bpy})$ complex-containing mesoporous cellular silica foams ($\text{Ir}(\text{ppy})_2(\text{bpy})\text{-MCFs}$).

2.6. Catalytic durability test

In order to determine the catalyst durability, the $\text{Ir}(\text{ppy})_2(\text{bpy})\text{-MCFs}$ catalyst was allowed to settle down after each run of reactions and the clear supernatant liquid was decanted slowly. The residual solid catalyst was reused with fresh charge of MeCN solvent and the reactant for subsequent recycle runs under the same reaction conditions. The Iridium species leached off from the heterogeneous catalyst $\text{Ir}(\text{ppy})_2(\text{bpy})\text{-MCFs}$ was determined by ICP analysis.

3. Results and discussion

3.1. Fabrication of $\text{Ir}(\text{ppy})_2(\text{bpy})\text{-MCFs}$ catalyst

The protocol for the preparation of $\text{Ir}(\text{ppy})_2(\text{bpy})\text{-MCFs}$ material was shown in Scheme 1. First, the vinyl-tagged $[\text{Ir}(\text{ppy})_2(\text{bpy})]\text{PF}_6$ complex was synthesized by reacting $[(\text{ppy})_2\text{IrCl}]_2$ compound with 4-(But-3-en-1-yl)-4-methyl-2,2-bipyridine. Meanwhile, the thiol-functionalized mesocellular silica foams (SH-MCFs) was prepared by using MPTMS (3-Mercaptopropyltrimethoxysilane) as the SH-functional groups source and TEOS (Tetraethoxysilane) as the silica skeleton under the P123 surfactant-directed assembly process. Finally, the thiol-ene click reaction between SH-MCFs and vinyl-tagged $\text{Ir}(\text{ppy})_2(\text{bpy})$ complex was performed to give the corresponding $\text{Ir}(\text{ppy})_2(\text{bpy})\text{-MCFs}$ catalyst [42].

To investigate the synthetic conditions, we firstly optimized the properties of SH-MCFs support by changing the molar ratios of MPTMS and TEOS with 10%, 20% and 30%, respectively. Elemental analysis (Table 1) showed that the contents of sulfur element in the series of SH-MCFs samples were in the range of 3.8–7.4 wt%. Meanwhile, X-ray photoelectron spectroscopy (XPS) spectrum of the representative SH-MCFs-2 revealed that the binding energy of $\text{S } 2\text{p}_{2/3}$ was 163.3 eV, confirming that the sulfur species was presented as the thiol molecules (Figure S1) [43]. These results demonstrated the successful incorporation of SH-groups in MCFs materials by this one-step co-condensation

Table 1
Structural parameters and element analysis of SH-MCFs and $\text{Ir}(\text{ppy})_2(\text{bpy})\text{-MCFs}$ samples.

Sample	S_{BET} (m^2/g)	D _p (cell, nm)	D _p (window, nm)	V _p (cm^3/g)	S (wt.%)
SH-MCFs-1	557	33.8	4.3	1.74	3.8
SH-MCFs-2	429	33.1	3.5	1.18	5.3
SH-MCFs-3	280	31.8	3.3	0.68	7.4
$\text{Ir}(\text{ppy})_2(\text{bpy})\text{-MCFs}$	355	30.1	3.0	0.94	7.2

self-assembly process. As shown in Fig. 1, all the SH-MCFs-1, SH-MCFs-2 and SH-MCFs-3 samples exhibited the typical IV nitrogen adsorption-desorption isotherms with the predominant H_1 hysteresis loops at high relative pressure of $P/P_0 = 0.47\text{--}0.99$, which were characteristic of the open mesoporous cellular foam structure [44]. As listed in Table 1, the surface areas, cell pore sizes, window pore sizes and pore volumes of these samples were gradually decreased with the increasing amounts of MPTMS in the initial solution. This phenomenon was probably due to the addition of MPTMS partially disturbed the self-assembly of silicate molecules and the hydrophilic segment of P123 surfactant, leading to the decreased ordered degree of cellular foam structure [45]. On basis of these results, we chosen the SH-MCFs-2 as the support to immobilize the $[\text{Ir}(\text{ppy})_2(\text{bpy})]\text{PF}_6$ complex since it had the suitable surface area and pore size as well as the relatively large amount of thiol-functional groups. Next, we explored different solvents and the mass ratios between SH-MCFs-2 and the vinyl-tagged $[\text{Ir}(\text{ppy})_2(\text{bpy})]\text{PF}_6$ complex in the thio-ene click immobilization process. As a result, the Iridium loading of $\text{Ir}(\text{ppy})_2(\text{bpy})\text{-MCFs}$ that determined by ICP analysis was up to 0.14 mmol/g by using 100 mg SH-MCFs-2 and 50 mg vinyl-tagged $[\text{Ir}(\text{ppy})_2(\text{bpy})]\text{PF}_6$ complex, and CHCl_3 as the solvent (Table S1).

3.2. Characterization of $\text{Ir}(\text{ppy})_2(\text{bpy})\text{-MCFs}$ catalyst

The TGA curve (Figure S2) demonstrated that the decomposition of organic thiol groups in the SH-MCFs-2 sample occurred between 230

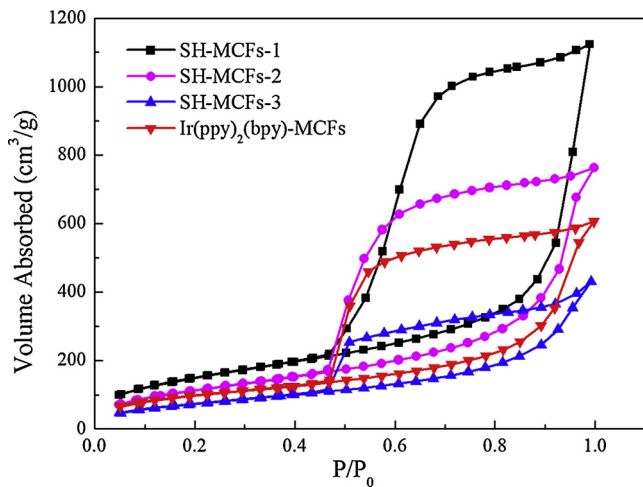


Fig. 1. Nitrogen sorption isotherms of SH-MCFs and $\text{Ir}(\text{ppy})_2(\text{bpy})\text{-MCFs}$ samples.

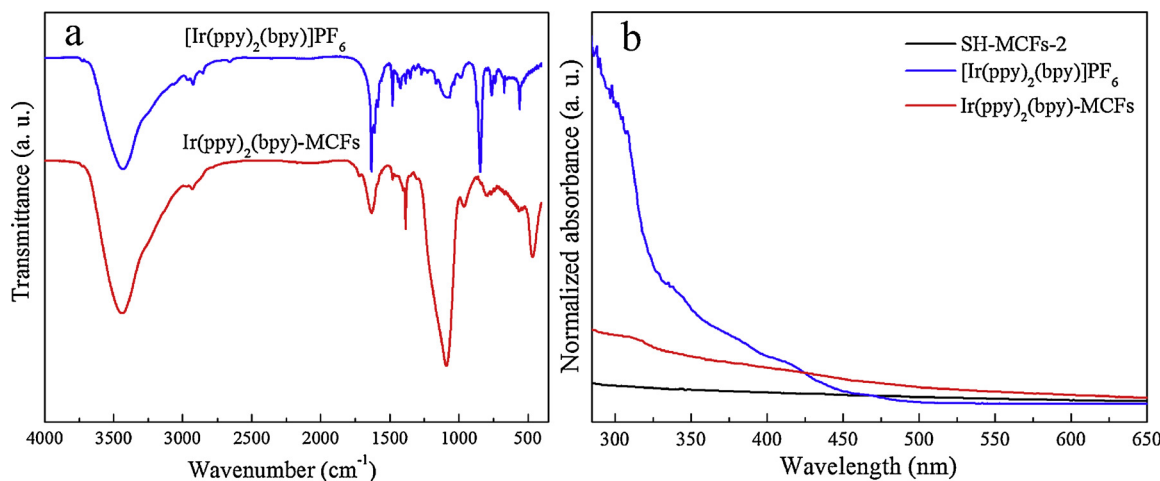


Fig. 2. (a) FT-IR spectra of $[\text{Ir}(\text{ppy})_2(\text{bpy})]\text{PF}_6$ and $\text{Ir}(\text{ppy})_2(\text{bpy})\text{-MCFs}$ and (b) UV-vis spectra of SH-MCFs-2, $[\text{Ir}(\text{ppy})_2(\text{bpy})]\text{PF}_6$ and $\text{Ir}(\text{ppy})_2(\text{bpy})\text{-MCFs}$ samples.

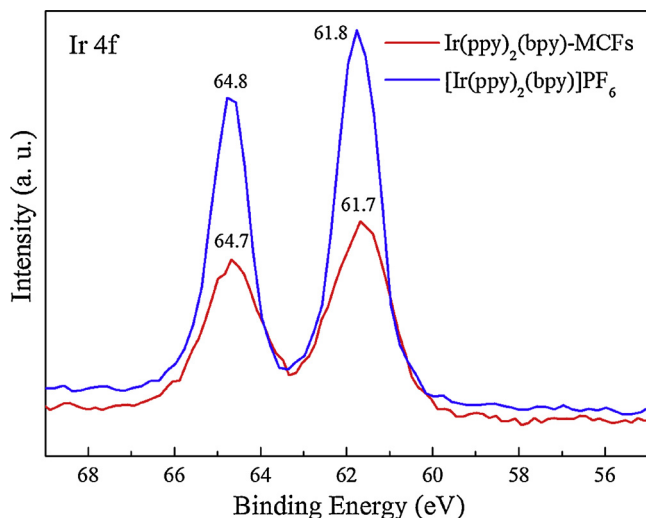


Fig. 3. Iridium XPS spectra of $[\text{Ir}(\text{ppy})_2(\text{bpy})]\text{PF}_6$ and $\text{Ir}(\text{ppy})_2(\text{bpy})\text{-MCFs}$ samples.

and 430 °C, which showed the weight loss of organic groups about 27%. For $\text{Ir}(\text{ppy})_2(\text{bpy})\text{-MCFs}$ sample, the additional weight loss with around 10% existed between 450 and 500 °C, which was attributed to the decomposition of $\text{Ir}(\text{ppy})_2(\text{bpy})$ complex [46]. FT-IR spectrum (Fig. 2a) of $\text{Ir}(\text{ppy})_2(\text{bpy})\text{-MCFs}$ sample displayed the major band centered at 1090 cm^{-1} indicative of Si-O-Si stretching mode. In addition, a series of bands in the regions of 1420–1470 and 1600–1630 cm^{-1}

corresponded to the ring stretching vibrations of the phenylpyridyl and bipyridine groups were observed [47]. Clearly, these bands were also found in the control $[\text{Ir}(\text{ppy})_2(\text{bpy})]\text{PF}_6$ complex. Meanwhile, UV-vis spectrum of $\text{Ir}(\text{ppy})_2(\text{bpy})\text{-MCFs}$ sample (Fig. 2b) exhibited the significant absorption enhancement from 300 to 500 nm in comparison with SH-MCFs support. It could be ascribed to the metal-to-ligand charge transfer (MLCT) transition [26], which was similar to that obtained for $[\text{Ir}(\text{ppy})_2(\text{bpy})]\text{PF}_6$ complex. Moreover, Iridium XPS spectra of $\text{Ir}(\text{ppy})_2(\text{bpy})\text{-MCFs}$ revealed that all the Iridium element presented in +3 oxidation state with the binding energy of 61.7 and 64.7 eV in Ir 4f_{7/2} and Ir 4f_{5/2} levels, respectively [34]. The data was in good accordance with that of the control $[\text{Ir}(\text{ppy})_2(\text{bpy})]\text{PF}_6$ complex (Fig. 3). Thus, it could be concluded that $\text{Ir}(\text{ppy})_2(\text{bpy})$ complex was successfully immobilized on the MCFs with the well-retained molecular configuration.

The porous structure of $\text{Ir}(\text{ppy})_2(\text{bpy})\text{-MCFs}$ could be analyzed by N₂ sorption isotherm and TEM image. As shown in Fig. 1, $\text{Ir}(\text{ppy})_2(\text{bpy})\text{-MCFs}$ still exhibited type IV isotherm with significant hysteresis loop in the relative pressure at $P/P_0 = 0.46\text{--}0.99$, indicating that it retained the porous structure of MCFs after the immobilization of $\text{Ir}(\text{ppy})_2(\text{bpy})$ complex [48]. The structure parameters including specific surface area, pore size and pore volume obtained from N₂ adsorption-desorption isotherms were listed in Table 1. After loading $\text{Ir}(\text{ppy})_2(\text{bpy})$ complex, the surface area reduced in parallel with the cell and window pore sizes as well as pore volume compared with SH-MCFs-2 support. It could be explained as the occupancy of Iridium complex in the pore channels of SH-MCFs-2. But, the average pore size only displayed the slight decrease, which revealed that the Iridium complex was homogeneously distributed in the inner channels rather than pore mouths [49]. Fig. 4

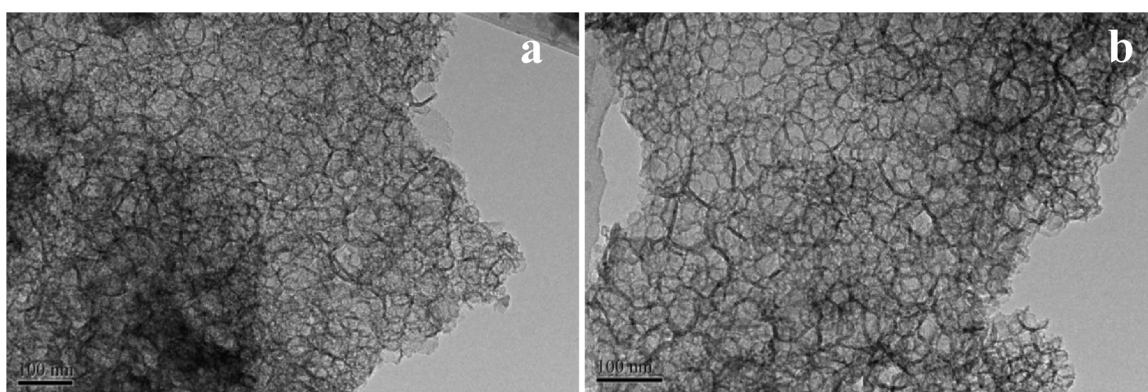


Fig. 4. TEM images of SH-MCFs-2 (a) and $\text{Ir}(\text{ppy})_2(\text{bpy})\text{-MCFs}$ (b) samples.

Table 2Catalytic performances of visible-light-driven depolymerization of oxidized lignin β -O-4 model compound under different reaction conditions.^a

Sample	Catalyst amount (mol%)	DIPEA amount (mmol)	HCOOH amount (mmol)	Conversion of A (%)	Yield of B (%)	Yield of C (%)
Ir(ppy) ₂ (bpy)-MCFs	1.0	1.0	1.0	17	11	10
Ir(ppy) ₂ (bpy)-MCFs	1.0	1.5	1.5	25	19	18
Ir(ppy) ₂ (bpy)-MCFs	1.0	2.0	2.0	27	21	20
Ir(ppy) ₂ (bpy)-MCFs	0.5	1.5	1.5	11	7	6
No light	1.0	1.5	1.5	trace	trace	trace
SH-MCFs	/	1.5	1.5	trace	trace	trace
No catalyst	/	1.5	1.5	trace	trace	trace

^a Reaction conditions: 0.50 mmol 2-(2-methoxyphenoxy)-1-(4-methoxyphenyl)ethanone, a certain amount of N,N-Diisopropylethylamine (DIPEA), HCOOH and catalyst, 5.0 mL MeCN, Xenon lamp (> 420 nm), 25 °C, 2.0 h.

Table 3Catalytic performances of visible-light-driven depolymerization of oxidized lignin β -O-4 model compound under different reaction time.^a

Catalyst	Reaction time (h)	Conversion of A (%)	Yield of B (%)	Yield of C (%)
Ir(ppy) ₂ (bpy)-MCFs	2	25	19	18
Ir(ppy) ₂ (bpy)-MCFs	3	57	53	52
Ir(ppy) ₂ (bpy)-MCFs	4	84	79	78
Ir(ppy) ₂ (bpy)-MCFs	5	95	88	87
Ir(ppy) ₂ (bpy)-MCFs	6	> 99	92	92
[Ir(ppy) ₂ (bpy)]PF ₆	6	> 99	96	96

^a Reaction conditions: 0.50 mmol 2-(2-methoxyphenoxy)-1-(4-methoxyphenyl)ethanone, 1.5 mmol N,N-Diisopropylethylamine (DIPEA), 1.5 mmol HCOOH and 1.0 mol% catalyst, 5.0 mL MeCN, Xenon lamp (> 420 nm), 25 °C.

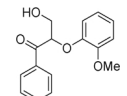
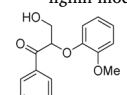
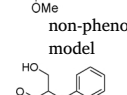
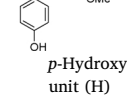
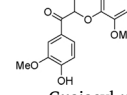
showed the TEM images of SH-MCF-2 and Ir(ppy)₂(bpy)-MCFs samples. They possessed the disordered mesoporous structure consistent with the opening foam-like structural features of typical mesostructured cellular foam materials. For Ir(ppy)₂(bpy)-MCFs, large mesopores with diameters ranging from 18 to 40 nm were observed, which further confirmed that the Iridium complex were loaded in the pore of SH-MCFs with well dispersion [50].

3.3. Catalytic performances of Ir(ppy)₂(bpy)-MCFs catalyst

We firstly used 2-(2-methoxyphenoxy)-1-(4-methoxyphenyl)ethanone as the oxidized lignin β -O-4 model compound to investigate the catalytic activity of Ir(ppy)₂(bpy)-MCFs catalyst. As shown in Table 2, it can efficiently catalyze the model molecule to the corresponding 4'-methoxyacetophenone and guaiacol after two hours visible-light illumination in the presence of organic base (DIPEA) and hydrogen source (HCOOH). The control experiments including the absence of visible light and Ir(ppy)₂(bpy)-MCFs photocatalyst as well as the use of SH-MCFs-2 support instead of photocatalyst revealed that both visible-light illumination and Ir(ppy)₂(bpy)-MCFs were indispensable for the reaction. Next, we explored the amount of Ir(ppy)₂(bpy)-MCFs catalyst, DIPEA and HCOOH and the reaction time (Tables 2 and 3). The

2-(2-methoxyphenoxy)-1-(4-methoxyphenyl)ethanone can be completely converted to 4'-methoxyacetophenone and guaiacol with 96% yields by using 1.0 mol% photocatalyst, 3.0 equiv. DIPEA and HCOOH additives after 6.0 h in 5.0 mL MeCN solvent. These results indicated that the fragments of the oxidized lignin β -O-4 model were obtained by photo-induced C_{B-O} bond scission [20]. Interestingly, it exhibited almost the same catalytic conversion and selectivity as that of homogeneous catalyst [Ir(ppy)₂(bpy)]PF₆ complex. This phenomenon demonstrated that Ir(ppy)₂(bpy)-MCFs catalyst retained the molecular configuration of Ir(ppy)₂(bpy) active species while it efficiently decreased the mass transfer resistance and the photon propagation

Table 4Comparison of catalytic performances of heterogeneous Ir(ppy)₂(bpy)-MCFs catalyst and homogeneous [Ir(ppy)₂(bpy)]PF₆ catalyst for different oxidized lignin β -O-4 model compounds.^a

Compound	Reaction Time (h)	Yield of B (%)		Yield of C (%)	
		Homo-Ir ^b	Hetero-Ir ^c	Homo-Ir ^b	Hetero-Ir ^c
	6	96	92	96	92
	6	98	96	97	93
	6	96	93	95	88
	7	95	93	95	91
	7	97	95	97	90

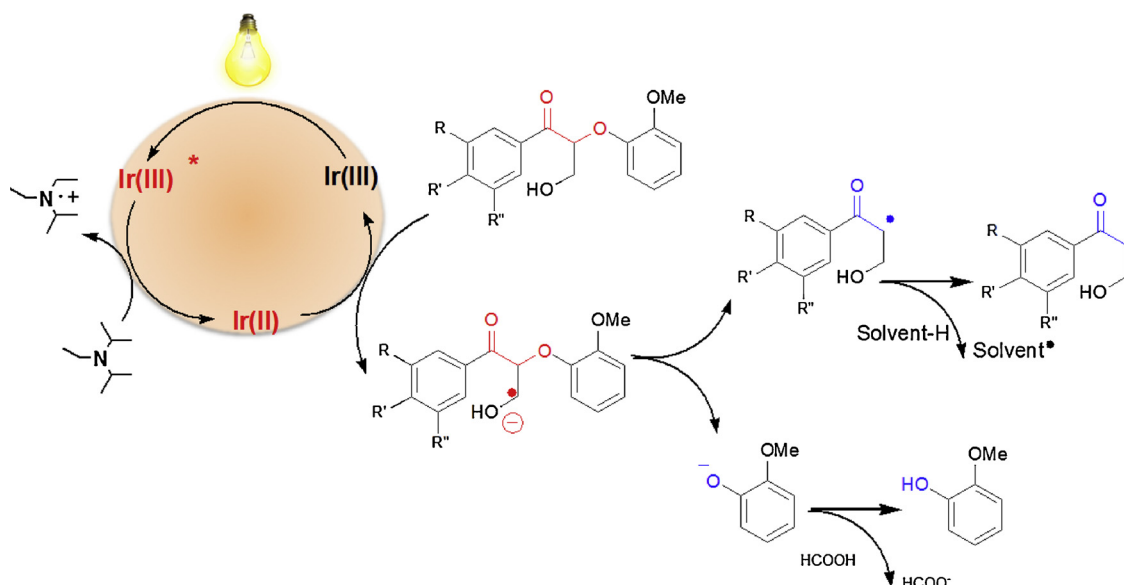
^a Reaction conditions: 0.50 mmol compound, 1.5 mmol N,N-Diisopropylethylamine (DIPEA), 1.5 mmol HCOOH and 1.0 mol% catalyst, 5.0 mL MeCN, Xenon lamp (> 420 nm), 25 °C.

^b Homo-Ir: Ir(ppy)₂(bpy)-MCFs.

^c Hetero-Ir: [Ir(ppy)₂(bpy)]PF₆.

hindrance by virtue of large surface area, open foam-like mesoporous structure and high visible-light transparency [40].

To verify that the current photocatalytic process was due to mesoporous silica supported Iridium complex rather than the leached



Scheme 2. Plausible mechanism for the $\text{Ir}(\text{ppy})_2(\text{bpy})$ -MCFs catalyzed visible-light-driven catalytic depolymerization of oxidized lignin β -O-4 model compound.

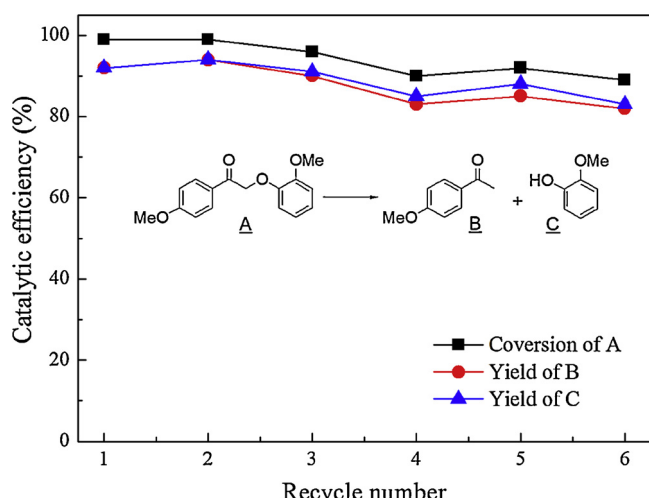


Fig. 5. Recycling tests of during visible light-mediated depolymerization of oxidized lignin β -O-4 model compound. Reaction conditions were shown in Table 3.

Iridium active species from the support in the reaction solution, the hot filtration experiment was carried out. $\text{Ir}(\text{ppy})_2(\text{bpy})$ -MCFs catalyst was filtered from the reaction mixture after 3.0 h until the conversion of 2-(2-methoxyphenoxy)-1-(4-methoxyphenyl)ethanone reached to around 60%, the reaction was continued for another 3.0 h under the same reaction conditions. The result indicated that no remarkable change in the conversion of 2-(2-methoxyphenoxy)-1-(4-methoxyphenyl)ethanone or the increased yields of 4'-methoxyacetophenone and guaiacol was observed. This phenomenon ruled out the possibility of the leaching homogeneous $\text{Ir}(\text{ppy})_2(\text{bpy})$ complex as the real active sites [51]. Moreover, this result was consistent with ICP-AES analysis, which revealed that the very low amount of Iridium element (less than 2.0 ppm) was detected in the reaction mixture while $\text{Ir}(\text{ppy})_2(\text{bpy})$ -MCFs catalyst was filtered out.

Furthermore, we investigated the generality of our heterogeneous photocatalytic strategy by testing other oxidized lignin β -O-4 model compounds, including those derived from *p*-hydroxyphenyl (H)-, guaiacyl (G)- and syringyl (S)-type lignin units (Table 4) [18]. The methoxy-substituted lignin β -O-4 compound offered $\text{C}_{\beta-\text{O}}$ bond cleavage products with high yields of 92–94% in 8.0 h. Next, we found that the oxidized lignin model with different substitution groups either methoxy or hydroxyl in the benzene ring did not obviously influence catalytic

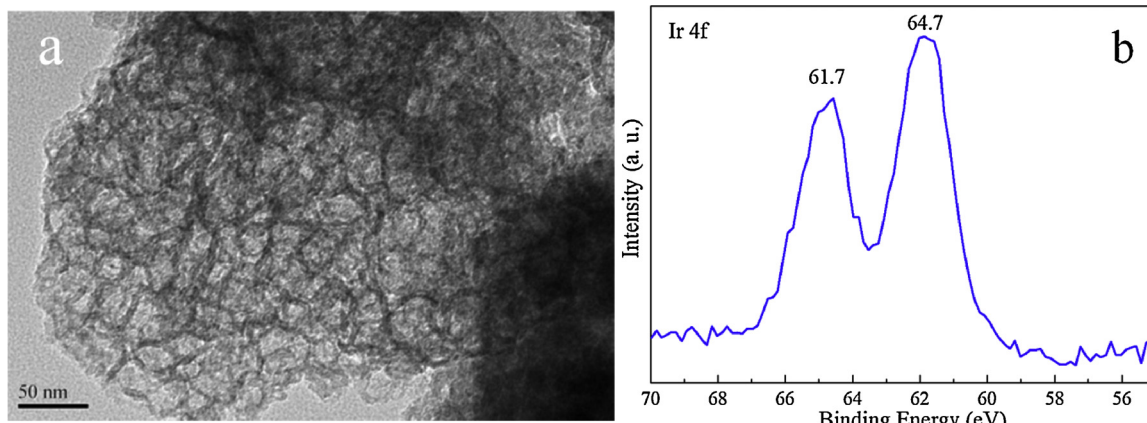


Fig. 6. TEM image (a) and Ir XPS spectrum (b) of the $\text{Ir}(\text{ppy})_2(\text{bpy})$ -MCFs catalyst after being reused six times.

performances. The yields of the corresponding ketones and guaiacols were in the range of 93–95%. Meanwhile, heterogeneous Ir(ppy)₂(bpy)-MCFs catalyst exhibited almost the same yields as that of homogeneous [Ir(ppy)₂(bpy)]PF₆ catalyst for all these representative reactants. These results provided the good potential for the future application in the depolymerization of the oxidized lignin polymer.

On basis of our results and the previously reported publication by Stephenson group [16,20], the postulated reaction mechanism of Ir(ppy)₂(bpy)-MCFs catalytic oxidized lignin β -O-4 model compound depolymerization was proposed (**Scheme 2**). Ir(ppy)₂(bpy)-MCFs catalyst adsorbs visible light induced the metal-to-ligand charge transfer to generate the [Ir(ppy)₂(bpy)]^{3+*} excited state. It can accept an electron from DIPEA to produce the reductive [Ir(ppy)₂(bpy)]²⁺ complex, which performed a single electron transfer to the benzylic ketone group in the oxidized lignin lignin β -O-4 model compound. This step is the rate determining step since it is mainly limited by the substance concentration and the excitation rate. Next, the generated radical anion undergoes a C _{α} -C _{β} bond cleavage to generate an alkoxy anion and the corresponding C _{α} -radical. Finally, the protonation of the alkoxy anion and the H-atom abstraction by C _{α} -radical produced the final ketone and phenolic products, respectively.

We also tested the recyclability of Ir(ppy)₂(bpy)-MCFs photocatalyst in the visible-light-catalyzed oxidized lignin model compound depolymerization reaction using 2-(2-methoxyphenoxy)-1-(4-methoxyphenyl) ethanone as the reactant. As shown in **Fig. 5**, Ir(ppy)₂(bpy)-MCFs could be reused at least six times without significant loss of catalytic efficiency. TEM image (**Fig. 6a**) showed that it preserved the typical mesoporous cellular foam structure. Also, ICP analysis revealed that Iridium content in the recycled Ir(ppy)₂(bpy)-MCFs photocatalyst remained almost the same (0.13 mmol/g). This phenomenon could be attributed to the existence of the stable carbon-sulfur bonding linkage between the Ir(ppy)₂(bpy) complex and the silica framework [52], which could effectively inhibit Ir(ppy)₂(bpy) complex leaching in the reuse and recycle processes. Furthermore, Ir XPS result (**Fig. 6b**) revealed the Ir coordination environment was unchanged since the same binding energy was the same with the fresh Ir(ppy)₂(bpy)-MCFs. These results confirmed that the Ir(ppy)₂(bpy)-MCFs catalyst could retain the physic-chemical properties after being used repetitively for six times, which was responsible for its excellent stability.

4. Conclusions

In summary, we developed a unique and simple click chemistry approach for the preparation of mesoporous cellular silica foams immobilized Ir(ppy)₂(bpy) complex by using the thiol-functionalized mesoporous cellular silica foams as the support and the vinyl-tagged [Ir(ppy)₂(bpy)]PF₆ complex as the active building block. The obtained Ir(ppy)₂(bpy)-MCFs visible-light photocatalyst showed high catalytic efficiency in the depolymerization of oxidized lignin β -O-4 model compounds under mild reaction conditions. In addition, it could be readily recycled by the filtration and reused without significant loss of its catalytic performances in a six times run test. The novel synthetic route is of great potential in the facile synthesis of high active and stable artificial photocatalytic systems for various visible-light-driven chemical transformations.

Acknowledgments

This work is supported by National Nature Science Foundation of China (51273112), Ministry of Education of China (PCSIRT_IRT_16R49), International Joint Laboratory on Resource Chemistry (IJLRC), and the Program for Professor of Special Appointment (Eastern Scholar) at Shanghai Institutions of Higher Learning (TP2016034).

Appendix A. Supplementary data

Supplementary material related to this article can be found, in the online version, at doi:<https://doi.org/10.1016/j.apcatb.2018.05.072>.

References

- [1] J.C. Serrano-Ruiz, J.A. Dumesic, Energy Environ. Sci. 4 (2011) 83.
- [2] M.S. Holm, S. Saravananurugan, E. Taarning, Science 328 (2010) 602.
- [3] Z.H. Sun, B. Fridrich, A. de Santi, S. Elangovan, K. Barta, Chem. Rev. 118 (2018) 614.
- [4] C.Z. Li, X.C. Zhao, A.Q. Wang, G.W. Huber, T. Zhang, Chem. Rev. 115 (2018) 11559.
- [5] S. Gillet, M. Aguedo, L. Petitjean, A.R.C. Morais, A.M. da Costa Lopes, R.M. Łukasik, P.T. Anastas, Green Chem. 19 (2017) 4200.
- [6] T. Yoshikawa, S. Shinohara, T. Yagi, N. Ryumon, Y. Nakasaka, T. Tago, T. Masuda, Appl. Catal. B 146 (2014) 289.
- [7] A. Toledano, L. Serrano, A. Pineda, A.A. Romero, R. Luque, J. Labidi, Appl. Catal. B 145 (2014) 43.
- [8] F. Yan, R. Ma, X.L. Ma, K. Cui, K. Wu, M.M. Chen, Y.D. Li, Appl. Catal. B 202 (2017) 305.
- [9] R.E. Key, J.J. Bozell, ACS Sustain. Chem. Eng. 4 (2016) 5123.
- [10] L. Chen, T.I. Korányi, E.J.M. Hensen, Chem. Commun. 52 (2016) 9375.
- [11] B. Joffres, M.T. Nguyen, D. Laurenti, C. Lorentz, V. Souchon, N. Charon, A. Daudin, A. Quignard, C. Geantet, Appl. Catal. B 184 (2016) 153.
- [12] M. Oregui-Bengoechea, I. Gandarias, N. Miletic, S.F. Simonsen, A. Kronstad, P.L. Arias, T. Barth, Appl. Catal. B 217 (2016) 353.
- [13] J.C. Colmenares, R.S. Varma, V. Nair, Chem. Soc. Rev. 46 (2017) 6675.
- [14] K.Y. Nandiwale, A.M. Danby, A. Ramanathan, R.V. Chaudhari, B. Subramaniam, ACS Sustain. Chem. Eng. 5 (2017) 7155.
- [15] J. Zakzeski, P.C.A. Bruijninx, A.L. Jongerius, B.M. Weckhuysen, Chem. Rev. 110 (2010) 3552.
- [16] I. Bosque, G. Magallanes, M. Rigoulet, M.D. Kärkäs, C.R.J. Stephenson, ACS Cent. Sci. 3 (2017) 621.
- [17] A. Rahimi, A. Azarpira, H. Kim, J. Ralph, S.S. Stahl, J. Am. Chem. Soc. 135 (2013) 6415.
- [18] A. Rahimi, A. Ulbrich, J.J. Coon, S.S. Shannon, Nature 515 (2014) 249.
- [19] J.Z. Bloh, R. Marschall, Eur. J. Org. Chem. 15 (2017) 2085.
- [20] J.D. Nguyen, B.S. Matsuura, C.R.J. Stephenson, J. Am. Soc. Chem. 136 (2014) 1218.
- [21] J. Luo, J. Zhang, J. Org. Chem. 81 (2016) 9131.
- [22] N.C. Luo, M. Wang, H. Li, J. Zhang, H.F. Liu, F. Wang, ACS Catal. 6 (2016) 7716.
- [23] N.C. Luo, M. Wang, H.J. Li, J. Zhang, T.T. Hou, H.J. Chen, X.C. Zhang, J.M. Lu, F. Wang, ACS Catal. 7 (2017) 4571.
- [24] J. Chen, W.X. Liu, Z.P. Song, H.L. Wang, Y.M. Xie, BioEnergy Res. 11 (2018) 166.
- [25] H. Mamlouk, J. Suriboot, P.K. Manyam, A. AlYazidi, D.E. Bergbreiter, S.T. Madrahimov, Catal. Sci. Technol. 8 (2018) 124.
- [26] S.B. Zhang, H. Wang, M. Li, J.Y. Han, S. Inagaki, X. Liu, Dalton Trans. 46 (2017) 9369.
- [27] X. Liu, Y. Maegawa, Y. Goto, K. Hara, S. Inagaki, Angew. Chem. Int. Ed. 55 (2016) 7943.
- [28] K. Tamura, A. Yamagishi, T. Kitazawa, H. Sato, Phys. Chem. Chem. Phys. 18 (2015) 18288.
- [29] W.J. Yoo, S. Kobayashi, Green Chem. 16 (2014) 2438.
- [30] D. Rackl, P. Kreitmeyer, O. Reiser, Green Chem. 18 (2016) 214.
- [31] F. Peng, P. Zhi, H. Ji, H. Zhao, F.Y. Kong, X.Z. Liang, Y.M. Shen, RSC Adv. 7 (2017) 19948.
- [32] B. An, L.Z. Zeng, M. Jia, Z. Li, Z.K. Lin, Y. Song, Y. Zhou, J. Cheng, C. Wang, W.B. Lin, J. Am. Chem. Soc. 139 (2017) 17747.
- [33] C. Wang, Z.G. Xie, K.E. deKrafft, W.B. Lin, ACS Appl. Mater. Interfaces 4 (2012) 2288.
- [34] S.B. Zhang, H. Wang, M. Li, J.Y. Han, X. Liu, J.L. Gong, Chem. Sci. 8 (2017) 4489.
- [35] P. Schmidt-Winkel, W.W. Lukens Jr., P.D. Yang, D.I. Margolese, J.S. Lettow, J.Y. Ying, G.D. Stucky, Chem. Mater. 12 (2000) 686.
- [36] L. Wei, Y.X. Zhao, Y.H. Zhang, C.C. Liu, J.P. Hong, H.F. Xiong, J.L. Li, J. Catal. 340 (2016) 205.
- [37] J. Wisniewska, M. Ziolek, N. Artioli, M. Daturi, J. Catal. 336 (2016) 58.
- [38] K. Stawicka, A.E. Díaz-Alvarez, V. Calvino-Casilda, M. Trejda, M.A. Bañares, M. Ziolek, J. Phys. Chem. C 120 (2016) 16699.
- [39] O. Verho, A. Nagendiran, C.W. Tai, E.V. Johnston, J.E. Bäckvall, ChemCatChem 6 (2014) 205.
- [40] D.Y. Qi, M.Y. Xing, J.L. Zhang, J. Phys. Chem. C 118 (2014) 7329.
- [41] G. Zhang, J. Yi, J. Shim, J. Lee, W. Choi, Appl. Catal. B 102 (2011) 132.
- [42] C.E. Hoyle, C.N. Bowman, Angew. Chem. Int. Ed. 49 (2010) 1540.
- [43] D.G. Castner, Langmuir 12 (1996) 5083.
- [44] L. Wolski, I. Sobczak, M. Ziolek, Microporous Mesoporous Mater. 243 (2017) 339.
- [45] C.M. Kang, J.L. Huang, W.H. He, F. Zhang, J. Organomet. Chem. 695 (2010) 120.
- [46] C.Y. Sun, X.L. Wang, X. Zhang, C. Qin, P. Li, Z.M. Su, D.X. Zhu, G.G. Shan, K.Z. Shao, H. Wu, J. Li, Nat. Commun. 4 (2013) 2717.
- [47] S. Ladouceur, D. Fortin, E. Zysman-Colman, Inorg. Chem. 49 (2010) 5625.
- [48] J. Shah, T.J. Pinnavaia, Chem. Mater. 17 (2005) 947.
- [49] K. Nakajima, I. Tomita, M. Hara, S. Hayashi, K. Domen, J.N. Kondo, Adv. Mater. 17 (2005) 1839.
- [50] F. Zhang, X.S. Yang, F.X. Zhu, J.L. Huang, W.H. He, W. Wang, H.X. Li, Chem. Sci. 3 (2012) 476.
- [51] X.Y. Li, Z.K. Hao, F. Zhang, H.X. Li, ACS Appl. Mater. Interfaces 8 (2016) 12141.
- [52] S. Kumari, B. Malvi, A.K. Ganai, V.K. Pillai, S.S. Gupta, J. Phys. Chem. C 36 (2011) 17774.